Emerging imaging methods to study whole-brain function in rodent models

Marija Markicevic [a,c], Iurii Savvateev [a,b,c], Christina Grimm [a,c], Valerio Zerbi [a, c]

[a] Neural Control of Movement Lab, HEST, ETH Zürich, Auguste-Piccard-Hof 1, 8093 Zurich, Switzerland
[b] Decision Neuroscience Lab, HEST, ETH Zürich, Winterthurerstrasse 190, 8057 Zurich, Switzerland
[c] Neuroscience Center Zurich, University and ETH Zurich, Winterthurerstrasse 190, 8057 Zurich, Switzerland

Corresponding author:
Dr. Valerio Zerbi
Neural Control of Movement Lab
Department of Health Sciences and Technology
ETH Zürich, Switzerland
Auguste-Piccard-Hof 1, 8093 Zurich
Phone: +41 44 633 29 37
valerio.zerbi@hest.ethz.ch

Key words: functional imaging, whole-brain function, rodents, functional MRI, functional ultrasound, photoacoustic, intrinsic optical imaging, microscopic imaging

Abstract

In the past decade, the idea that single populations of neurons support cognition and behavior has gradually given way to the realization that connectivity matters, and that complex behavior results from interactions between remote yet anatomically connected areas that form specialized networks. In parallel, innovation in brain imaging techniques has led to the availability of a broad set of imaging tools to characterize the functional organization of complex networks. However, each of these tools poses significant technical challenges and faces limitations, which require careful consideration of their underlying anatomical, physiological and physical specificity. In this review, we focus on emerging methods for measuring spontaneous or evoked activity in the brain. We discuss methods that can measure large-scale brain activity (directly or indirectly) with relatively high temporal resolution, from milliseconds to seconds. We further focus on methods designed for studying the mammalian brain in preclinical models, specifically in mice and rats. This field has seen a great deal of innovation in recent years, facilitated by concomitant innovation in gene editing techniques and the possibility of more invasive recordings. This review aims to give an overview of currently available preclinical imaging methods and an outlook on future developments. This information is suitable for educational purposes and for assisting scientists in choosing the appropriate method for their own research question.

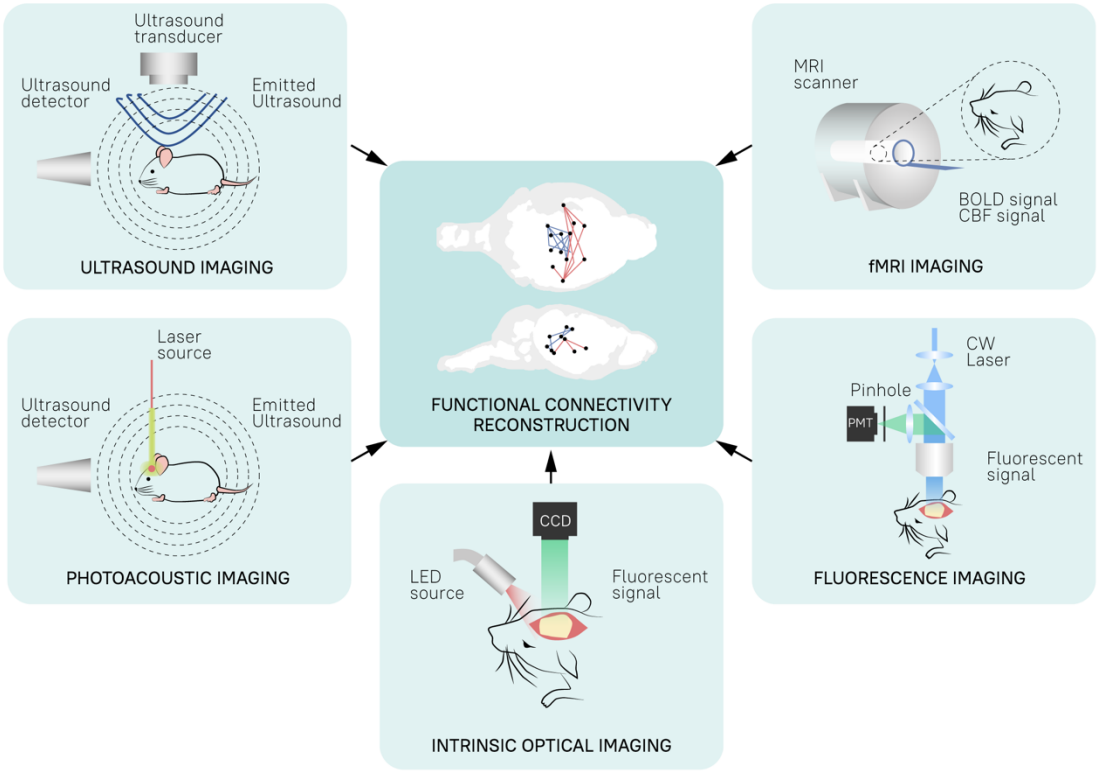

Introduction

Galaxies of thought, cognition and movement. The observation of natural phenomena is the basis of modern scientific thought, and a common approach to all scientific disciplines, from astronomy to neuroscience. Through observations we can generate, confirm, extend or challenge theories and models of how nature works. And just as telescopes are the means of unlocking the secrets of outer space, our understanding of the brain depends on the methods we use to observe its constituent elements and study how they interact with each other, creating galaxies of thought, cognition and movement. While there is no single technique (yet) capable of observing all these phenomena, there are many technologies at our disposal to study brain activity across multiple temporal and spatial dimensions (**Figure 1**).

The basic substrate used by the brain to transmit information is represented by electrical events called neuronal spikes and the release of chemical neurotransmitters in the synaptic terminals. Decades of (electro)physiological research facilitated by *in-vitro* preparations, neuronal cell cultures or organoids, and *in-vivo* recordings have advanced our understanding of the mechanisms that drive neurons to fire and transmit their signals through the network. While neuronal rhythmicity plays an essential role in facilitating information processing across spatial and temporal hierarchies in the brain[1], individual neural spikes per se are too weak to influence complex behaviour (with notable exceptions)[2]. If our cognition really depended on individual spikes, we would deal with a poorly defined, high-dimensional system, not suitable for life. According to this view, correlates between the activity of a single neuron and a specific cognitive process provide a limited description of the causal relationship between brain activity and behaviour[3]. Thus, it seems increasingly likely that the brain does not use actual spike coding but population - or neural ensembles - coding that unfold on a limited, low-dimensional portion of the full neural space[4,5]. As information flows through the brain, population activity is further integrated into large-scale networks via the *connectome*[6]. The result is that large numbers of brain regions are active during every aspect of cognition and behaviour.

Since one of the more tractable goals of quantitative neuroscience is to develop predictive models that relate brain activity to behaviour, observing activity and dynamics in neural networks – possibly in multiple brain areas – can get us closer to this goal. To do that, scientists and engineers have developed an array of methods capable of looking at whole-brain activity from a zoomed-out perspective. In this review, we aim to provide the reader with an overview of the emerging methods for observing system and network-level brain function in rodents. While this article is not designed to provide a full review of the literature, history and physics behind each method, we distil the nature and the unique features of each technique, and comment on their use and potential for future expansion and of course, their limitations. We wrote this article for scientists who want to expand their view on preclinical imaging methods, are looking for the appropriate method to address their research question, and for didactical purposes.

Functional MRI

Functional Magnetic Resonance Imaging (fMRI) is one of the leading techniques to study whole-brain function in humans. Its first description dates back to the early 1990s, when Ogawa and colleagues[7] described the principles of blood oxygen level-dependent (BOLD) magnetic resonance imaging (MRI): local changes in neuronal activity require a dynamic supply of oxygen and glucose, provided by a highly dense vascular system. More specifically, the process of neurovascular coupling, which entails the acute regulation of cerebral blood flow (CBF) via vasoactive molecules and neural messengers, ensures that this change in energetic demand is met (extensively reviewed in [8-11]). To this day, much research effort is directed to the identification of cellular and molecular messengers that communicate neuronal activity to the vasculature, helping us understand cerebrovascular regulation and more accurately interpret observed fMRI signals[12-17]. Ultimately, regional alterations in CBF influence the ratio of oxygenated vs

deoxygenated haemoglobin, whose distinct magnetic properties give rise to the BOLD signal. It is the paramagnetic properties of the deoxyhaemoglobin that cause magnetic susceptibility inside blood vessels and surrounding tissue, thus affecting the magnetic field and the spin-spin relaxation time (T2 / $T2^*$).

MRI sequences that are sensitive to the $T2^*$, such as gradient-echo (GRE) echo planar imaging (EPI), are often used for studying the fast dynamics of hemodynamic responses with a spatial resolution of ~1 to 3mm and with a temporal resolution of ~1 to 3 seconds[18,19]. In 1995 Biswal et al.[20] showed that also slow (<0.1 Hz), spontaneous fluctuations of the BOLD signal measured during rest periods (i.e. without the overt perceptual input or motor output typically present in traditional task-based fMRI studies) could be measured with a GRE-EPI sequence. These fluctuations form spatial patterns of correlated activity (i.e. networks) that unfold along the long-range axonal connections of the brain, revealing its intrinsic functional architecture[21]. Since then, resting-state fMRI (rsfMRI) has become the method of choice to map regional interactions that occur in a resting or task-negative state across the whole brain in humans (with ~16.000 rsfMRI papers published in the past two decades; source: Pubmed, Jan 2021). To this day, GRE-EPI sequences with intrinsically high $T2^*$ sensitivity, high temporal resolution and signal stability, are the most common choice for BOLD fMRI. It should be noted, though, that few technical caveats of the $T2^*$ contrast remain[22]. In fact, GRE sequences are more frequently troubled by susceptibility and chemical shift artifacts given their high sensitivity to large vessels, potentially leading to overestimations of activated regions[22,23]. However, there are other types of MRI sequences that can work around these problems. The most common are T2-weighted techniques such as EPI spin-echo (SE) sequences, which filter signals associated with larger veins and enhance contrast from small capillaries that are more likely to be closer to the site of neuronal activity[24]. This advantage comes at the expense of lower BOLD sensitivity and longer acquisition times[25,26]. Given that different techniques of contrast weighting are likely to involve different trade-offs between sensitivity and spatial specificity of the observed fMRI responses, making an informed decision regarding the choice of MRI pulse sequence to best fit one's research question and study design is advisable.

Rodent functional MRI

While the evidence provided by fMRI imaging in humans continues to teach us a lot about brain-behaviour relationships, studying the biological underpinnings which underlie large-scale networks and dynamics requires interventional and controlled experimental conditions only achievable in animal models. The past 10 years have seen a rapid increase in studies applying rsfMRI in rodent models. Early work mapped the spatial extent of resting-state networks in rats[27-30] and mice[31]. These findings have led to the realization that the rodent brain is organized in large-scale networks, the properties of which are similar to those reported in humans. This laid the foundation for studying the rodent brain using multiple approaches adapted from the human literature, such as independent component analysis[32-35], seed-based correlation[33,36-39], dynamic functional connectivity analysis[40-42] and tools from graph theory[43,44]. Other work focused on the relationship between network function and neuronal axonal connectivity, for example by comparing rsfMRI data with the underlying anatomical connectivity from tracer injection experiments by the Allen Institute[45]. Thanks to this work, we have learned that high functional connectivity emerges predominantly between monosynaptically connected regions in the cortex, albeit this relation is not always present in subcortical regions like the thalamus[46]. In another study, Mills and colleagues showed that, in addition to neuro-anatomical wiring, the genetic profiles of individual brain regions strongly contribute to functional connectivity, and that the variance of fMRI signals is best explained by a linear combination of axonal and gene expression data[47].

Rodent fMRI has also been used to better elucidate the mechanism of BOLD, for example by combining it with direct measurement of neural and astrocytic activity[48-52]. Schlegel and colleagues[48] performed sensory-evoked (hind-paw stimulation) astrocytic and neuron specific calcium recordings with simultaneous BOLD-fMRI, and showed strong correlations between BOLD and calcium signals (both neuronal and astrocytic). Similarly, Tong and colleagues[50] revealed a strong coupling between the neuronal calcium signal and task-based and task-free BOLD responses.

Given that rodent and human fMRI share the same sequences for signal generation and use the same (pre)processing techniques, the technique holds great promise to understand the biological basis of human pathologies and link those with clinical outcomes in patients. Genetically modified (transgenic) animal models provide a crucial advantage in this undertaking. An extensive list of transgenic models has been investigated using rsfMRI to study numerous neuropsychological conditions, including Alzheimer's disease[53-55], schizophrenia[56], pain[57] and autism[58-60,61]. For example, a recent study mapped the connectivity changes in subjects with autism-associated 16p11.2 deletion and in the mouse model with the same genetic mutation. Both groups displayed diminished functional connectivity in allegedly homologous brain networks[44]. In this context, fMRI represents a valuable tool for addressing the growing need to formally identify common brain circuits between rodents and humans to determine the scope and limits of rodent translational models[62,63]. One caveat is that rodent fMRI is usually carried out in the anesthetized state to minimise head-motion during scanning, and only a handful of labs are acquiring fMRI data in awake animals[15,64,65]. The choice of anaesthetic introduces confounds in fMRI measurements and is certainly a limitation for translating findings to humans[38,39].

New Avenues

New acquisition sequences to assess brain function with MRI are emerging at an ever-increasing rate. A family of MRI methods assess brain activity in rodents (other than BOLD) by measuring cerebral blood volume (CBV) and CBF, usually referred to as *perfusion MRI*. CBV and / or CBF are often measured by injecting a paramagnetic contrast agent (CA) into the bloodstream[66]. The CA's passage causes transient magnetic field inhomogeneities and introduces phase distortion of the water proton spins resulting in changes in T1, T2 or $T2^*$ relaxation times, which can be captured with different MRI sequences. Commonly used CAs are paramagnetic gadolinium chelates, which increase T1, and superparamagnetic iron oxide nanoparticles, which decrease $T2/T2^*$ (for a thorough review of techniques of perfusion MRI and comparison of CA see[66-68]). CBV-weighted fMRI in small animals has some advantages over BOLD measurements, including higher signal-to-noise ratio (SNR) and reduced susceptibility artefact. Furthermore, CBV represents a direct and easily interpretable component of the neurovascular cascade compared to the BOLD signal[66]. CBV-fMRI in combination with chemogenetic or optogenetic neuromodulation has been used to study the influence of serotonergic transmission on brain function. Giorgi and colleagues[69] measured the effects of pharmacological and chemogenetic serotonin modulation on whole-brain CBV. Their results indicate that serotonin modulation change the CBV in multiple primary target regions of serotonin encompassing corticohippocampal and ventrostriatal areas. A similar study from Grandjean and colleagues[70] showed that optogenetic activation of the dorsal raphe nucleus resulted in a CBV decrease in primary target regions of serotonin. Additionally, inducing acute stress by forced immobilization prior to the MRI also decreased the CBV in the same dorsal raphe's primary target regions.

Other MRI sequences have been developed to achieve faster recordings, artifact-free images or increase the specificity of MRI responses in relation to the underlying neural signals. Compared to conventional fMRI sequences, ultrafast fMRI sequences aim to shorten the repetition time (TR), which is the time from the application of a radiofrequency excitation pulse to the application of the next pulse. This can be achieved in a number of ways. One approach is to use simultaneous multi-slice imaging. Recently, Lee and colleagues[71] developed a sequence for rodent fMRI that can encode multiple slices

simultaneously by using slice-select gradient blips. Blips impose different amounts of linear phase for different slices; thanks to an extended field of view (FOV), each slice is shifted towards a different and non-overlapping portion of the FOV, thus speeding up the acquisition by a factor of 4, while keeping a similar signal-to-noise ratio to conventional EPI sequences.

Being able to use high spatio-temporal resolution is also critical to discern the direction of information flow using the onset times of fMRI responses. For example, Jung and colleagues[72] applied a GRE-EPI sequence at ultra-high magnetic field (15.2 T) with a temporal resolution of 250ms and spatial resolution of 156x156x500μm^3 during either electrical paw stimulation or optogenetics stimulation of the motor cortex. Their results showed that the order of onset times varies between regions and active layers and coincides with their known sequence of neural activation. This work provided further evidence that ultra-high resolution BOLD MRI can be useful to identify bottom-up and top-down processes between cortico-cortical and cortico-thalamic regions and to assess the direction of information flow.

Images generated by conventional fMRI sequences in rodents suffer from a high sensitivity to magnetic susceptibility artifacts due to the high field of scanners and the relatively long echo time required to generate the BOLD contrast. To solve this problem, MacKinnon and colleagues combined a zero-time echo (ZTE) pulse sequence with iron oxide nanoparticles to acquire CBV. The ZTE sequence is characterized by a very short echo time, which means that signal acquisition occurs immediately after the radio frequency pulse, preventing signal decay. At the same time, iron oxide nanoparticles shorten the T1 relaxation time, resulting in the detection of CBV-weighted functional activations in the brain even with a low echo time. This allows for a three-fold increase in the magnitude of the signal-to-noise ratio, along with a reduction in susceptibility artifacts and acoustic noise[73].

New MRI sequences have also been developed to measure brain activity differently from the hemodynamic response. One example is given by diffusion functional imaging (dfMRI). In dfMRI, a spin-echo echo planar (SE-EPI) sequence is combined with an isotropic diffusion encoding (IDE) gradient, to impart isotropic diffusion-weighting contrast in the acquired signal. This makes dfMRI sensitive to rapid changes in three-dimensional tissue boundaries induced by neuronal activation[74,75]. Evidence from intrinsic optical signals (IOS) studies suggests a strong coupling between neural activity and microscopic (sub)cellular morphological changes[76]. Therefore, dfMRI was developed to detect changes in water diffusion properties related to "cell swelling" and coupled to neuronal activity rather than hemodynamic responses[74,77]. Nunes et al., [78] were the first to investigate in greater depth the mechanism underlying neuromorphological coupling by developing an ultrafast line-scanning dfMRI SE-EPI sequence with a time resolution of 100 ms, which enabled the detection of rapid diffusion dynamics. Upon forepaw stimulation, they detected in the rat somatosensory cortex that the dfMRI signal contains two different components: a fast-onset component that is insensitive to vascular change, followed by a slower component sensitive to vascular change. Independent IOS of optogenetically stimulated brain slices confirmed the close similarity between fast IOS and the fast-onset dfMRI component, thus suggesting further evidence of neuromorphological coupling. Moreover, in human studies, dfMRI showed higher spatial accuracy at activation mapping compared to classic functional MRI approaches[79 80]. Nunes and colleagues applied dfMRI in rodent fMRI, and tested the specificity of dfMRI by mapping whole-brain responses upon hind-paw stimulation with voxel resolution[81]. Their results indicated that the dfMRI signal exhibits layer specificity and is spatially overlapping with the underlying neural activity within the thalamocortical pathway.

Another family of methods that has recently been developed to evaluate neural activity is called molecular fMRI. Molecular fMRI monitors brain activity through the use of chemical or genetically-encoded probes i.e., MRI molecular imaging agents, which are designed to bind to specific molecular and cellular targets in the brain, analogous to fluorescent dyes for optical imaging[82-84]. These MRI molecular imaging agents work by interacting with water molecules to alter T1 and T2 relaxation times, or in some cases by incorporating nuclei that can be probed using radio frequencies distinct from those

used to measure water protons[83,85]. Thus, molecular fMRI readout reflects distinct molecular hallmark of neural activity, rather than hemodynamic coupling that underlies BOLD fMRI. The first molecular fMRI study to combine molecular specificity and spatial coverage using a neurotransmitter sensor detectable by MRI assessed dopamine signalling. They injected MRI contrast agent sensitive to dopamine into the rat nucleus accumbens (NAc) and measured changes in dopamine concentration in NAc and caudate putamen (CPu) upon electrical stimulation of the medial forebrain bundle in lateral hypothalamus[86]. Recently, this approach was combined with BOLD fMRI[87], where simultaneous functional BOLD and molecular imaging responses were recorded throughout the rat brain using multi-gradient echo MRI pulse sequence, during electrical stimulation of hypothalamus. Results indicated that phasic dopamine release in the NAc and medial CPu alters the duration, but not the magnitude, of the stimulus responses across the striatum via postsynaptic effects that vary across subregions, and that dopamine causally modulates BOLD fMRI responses in the distal cortical regions.

Another method that allows quantitative and noninvasive assessment of cerebral metabolism during brain activity is functional magnetic resonance spectroscopy (fMRS). The goal of fMRS is to obtain precise quantitative *in vivo* measurements of various metabolic concentration changes during brain activity. While broadly used in human brain studies, its application in rodents is still limited mainly due to low signal-to-noise ratio, low (~4sec) temporal resolution and anaesthesia confounds[88,89]. A recent review gives a detailed overview of the methodological aspects and translational prospects of fMRS in rodents[88].

Ultrasound imaging

Ultrasound imaging is a widely used diagnostic technique in medicine that is based on the principle of the emission of ultrasonic waves (from 20KHz to about 15MHz) and the transmission of echoes. Using the speed of sound and the time of each echo's return, an ultrasound system calculates the distance from the transducer to the tissue boundary and then uses this information to generate images of tissues and organs[90]. Ultrasound systems can also be tuned to assess blood flow using the Doppler effect. The principle of Doppler ultrasound consists of detecting the movement of red blood cells by repeating pulsed emissions and studying the temporal variations of subsequent backscattered signals[91]. In clinics, Doppler ultrasound is the most commonly used technique to study blood circulation in the heart, arteries, limbs, kidney, and liver. However, for the brain, the application of transcranial Doppler (TCD) ultrasound is limited due to strong attenuation of the ultrasound beam by the skull, and its only clinical use is to diagnose cerebrovascular pathologies in newborns through the fontanel (for a review of TCD applications see[92]).

Functional ultrasound imaging in rodents

Until recently, little work has been done in preclinical rodent neuroscience using TCD. While partial skull removal could resolve scattering problems, conventional ultrasound still suffers from low sensitivity, which limits its application to image blood volume or flow in major cerebral arteries. However, the development of new concepts and technologies, such as ultrafast ultrasound and the use of plane-wave illumination as opposed to focused beam scanning, have enabled the use of ultrasound in basic neuroscience research[93]. Thanks to new scanners capable of acquiring images at a very high frame rate (~20 kHz), ultra-fast ultrasound can boost the power Doppler signal-to-noise ratio over 50-fold, without the need of contrast agents[90]. This increased sensitivity allows mapping of blood flow changes in small arterioles (up to 1 mm/s) that are related to small and transient changes in neuronal activity, laying the foundation for functional ultrasound (fUS) imaging (for a review on the techniques and physics of this technology see[90] and[93]).

The first application of fUS imaging in translational neuroscience appeared in 2011, when Macé and colleagues showed the activation of the barrel cortex following whisker stimulation in anesthetised rats

with high spatio-temporal detail[94]. Furthermore, the authors measured the spatiotemporal dynamics of epileptiform seizures, showing cortical spreading depression propagating throughout the entire brain. Since then, more groups have started to use fUS as a tool to record whole-brain activity in many behavioural and cognitive tasks, such as forepaw electrical stimulation in rats[95], or at rest[96,97]. In most cases, large cranial windows or skull thinning procedures were used for stable chronic imaging of deep brain structures. However, in 2017 Tiran and colleagues showed that the whole brain vasculature could be imaged through the skull and skin in awake and freely moving mice, whereas young rats can be imaged up to 35 days of age without prominent reductions in image quality[98]. A year later, Macé et al used fUS to map the brain areas activated during optokinetic reflex in awake mice and functionally dissect the regions whose activity depended on the reflex's motor output[99]. To date, new strategies can further increase the resolution of acquired images while maintaining rapid acquisition, for example using microbubble contrast agents and time tracking of microbubble positions[100].
In general, brain imaging in awake and behaving animals confers an advantage to fUS over fMRI. Furthermore, fUS combines whole brain reading with relatively high spatial resolution (100 x 100 x 300 µm) but with higher temporal resolution and low operating and maintenance costs. Although the skull remains an obstacle in fUS imaging for ultrasound wave propagation, the use of contrast agents[101] or a surgical procedure to produce a craniotomy or thinned skull window can solve this problem. Thanks to recent developments in injectable ultrasound contrast media or ultrafast high SNR sequences, an expansion of preclinical fUS applications in neuroscience is expected in the near future.

Fluorescence imaging

There are several optical imaging techniques that measure the activity of single neurons or neural groups, based on voltage or calcium dyes or genetically encoded probes. More recently the field has seen strong development of methods that increase the visual field and allow large-scale measurements of neural activity. The basic principle common to these techniques lies in the light emission of specific chemical compounds named fluorophores. The fluorophore absorbs light of a specific wavelength that brings it from a ground state to an excited state. When the fluorophore relaxes back to the ground state, in a process named luminescence, it emits light at a specific wavelength and energy. The light emitted during the luminescence – the fluorescence signal – is then captured by the adjacent optical system. The two key factors defining a fluorescent imaging technique are (i) the type of a fluorophore used[102,103] and (ii) the design of the optical system[104]. In the following sections, we will address both factors with respect to *in-vivo* functional brain imaging in rodents.

Fluorophores

Fluorophores can change their fluorescent properties, such as the wavelength or the intensity of the fluorescent signal, when involved in a specific physiological process, e.g. the firing of an action potential. The two most popular families of fluorophores used for *in-vivo* brain imaging are (i) calcium and (ii) voltage indicators. Calcium indicators measure changes in intracellular calcium ion concentration, whereas voltage indicators assess alterations in the membrane potential.
Both calcium and voltage indicators can be further divided into two main groups: organic (e.g. chemical)[105-107] and genetically encoded[107,108]. Organic calcium (e.g. fluo-4) or voltage (e.g. ANINNE-6) indicators are synthesized organic molecules that are delivered into a target cell via bulk loading or cell microinjections[105,107,109,110]. In contrast, genetically encoded calcium (e.g. GCaMPs) or voltage (e.g. ASAPs) indicators are expressed directly by the target cell. The incorporation of the indicator genes is achieved by using transgenic animals and/or virus vectors designed to express the genetic material under the control of a tissue specific promoter[107-109,111]. The cell type specific expression ensured by a tissue specific promoter makes genetically encoded calcium indicators (e.g. GCaMPs) the most popular choice for *in-vivo* brain fluorescent imaging in rodents.

Voltage indicators are sensitive to subthreshold membrane voltage dynamics and have a higher temporal resolution in comparison to the calcium indicators[107,112] Nevertheless, their use for wide field *in-vivo* brain imaging in rodents is hampered by the intrinsic low SNR[109] and by the technical challenge of achieving a precise localization of the voltage indicators in the cell membrane[107,112]. Therefore, while recognizing recent developments[107,112] and the potential of multi-area voltage imaging[112], we will focus our review on calcium indicators.

Optical designs

There are several optical systems currently available for detecting the fluorescent signal emitted by a fluorophore. Each of these can be used to maximize certain image parameters such as: acquisition speed, spatial resolution, FOV and dimensionality (e.g. 2D slice or 3D image)[104]. In the next sections, we focus on the most common fluorescence imaging procedures used for *in-vivo* brain imaging in rodents. For each method, we explain the basic principles of the optical design and review work that demonstrates its application in studying brain function with a large FOV.

Wide-field fluorescence imaging

Wide-field fluorescence imaging (WF) refers to a procedure in which a whole specimen (e.g. the targeted brain regions or the entire cortex) is illuminated and the emitted fluorescence is recorded by a joined optical system (**Figure 2**). In WF, it is essential to guarantee the passage of light with minimal dispersion and absorption; for this reason, WF is often combined with a procedure to replace the skull with a glass cranial window[113,114]. For example, Kim and colleagues measured GCaMP fluorescent signals with single neuron resolution throughout the entire dorsal cortex in awake, head-fixed mice[114]. However, WF can also be conducted through the skull by removing only the scalp. This severely limits the precision and resolution of the images but also minimizes invasiveness. Using WF imaging of GCaMP through the intact skull, Peters and colleagues functionally mapped activity across the entire dorsal cortex in awake head-fixed mice, with a spatial resolution of 20 μm[115].

Animal experiments with head restraints impose a fundamental technical limit on the behaviour that can be studied. To overcome this limitation, WF micro-endoscopes and optical fibres have been designed to visualize cortical and subcortical activity in awake and freely moving animals[116-120]. De Groot and colleagues [120] integrated two micro-endoscopes for simultaneous recording from distant brain regions, an inertial measurement unit for movement monitoring and an LED driver for optogenetic stimulation in a single device named the "NINscope". In one of their demonstrations, NINscopes were used to record the fluorescence of GCaMPs from the cortex and cerebellum and study the generation of movement upon cerebellar optogenetic stimulation in freely moving mice.

Despite the great potential of WF for *in vivo* brain imaging, its optical design suffers from a strong susceptibility to background fluorescence caused by the signal coming out of the focal plane. This places some fundamental constraints on WF applications. First, the background fluorescence decreases the SNR, which limits the spatial resolution and does not allow scanning subcellular structures (eg. synaptic boutons). Second, since the depth of focus is determined by fixed parameters of the optics, there is greater blur in the image when targeting deeper structures due to the background signal from the regions above. This currently limits the depth of WF imaging to the superficial layers of cortex. Finally, the continuous excitation of fluorophores from outside the focal plane can lead to an increase in phototoxicity and the production of reactive oxygen species (ROS), and photobleaching, which results in the inactivation of the fluorophore.

Confocal fluorescence imaging

Confocal microscopes use the same optical scheme as WF but with two additional features in order to increase the SNR. First, confocal microscopes utilize a tiny diaphragm, named a "pinhole", to remove

the signal coming out of the focal plane. Second, confocal microscopes use lasers as a light source instead of LEDs or arc-lamps. This increases the focus of the illumination beam on the targeted region, while minimizing out of focus illumination. To achieve a large FOV, a complete 2D or 3D image of a sample is usually acquired by moving the illumination spot across the sample[104,109,121]. Confocal fluorescence imaging was used by Yoshida and colleagues[122] to measure GCaMP6 fluorescence from individual axonal boutons in behaving head-restrained mice. By using a multispot confocal design, they could image for the first time a relatively large FOV of 1mm^2. This allowed the study of long-range projecting axons from the thalamus to the primary motor cortex (M1) in layer 1. In order to circumvent the need for a head-fixation constraint, Dussaux and colleagues developed a fibrescope adaptation of the confocal design, which allows a FOV of 230µm with single cell spatial resolution. This design was used to study changes in the velocity of red blood cells in cortical micro vessels in freely behaving mice compared to anaesthetised animals[123]. Nevertheless, in the confocal design the photons out of the focal plane still contribute to phototoxicity and photobleaching[124]. Another drawback is related to tissue scattering, which limits the depth of focus to a maximum of 100-200µm[122,123].

Multiphoton fluorescence imaging

Multiphoton microscopes use two or three photons to provide the energy needed to excite a fluorophore. The use of multiple photons means that the individual energy of each photon will be lower than that of a single excitation photon. Therefore, the corresponding wavelengths are shifted in the red / infrared part of the light spectrum, which is less scattered by brain tissues than other wavelengths. This gives multiphoton fluorescence imaging a greater depth of penetration than one-photon modes (e.g. WF, confocal). Also, due to the greater focus of the laser beam, the fluorophores outside the focal plane do not absorb two photons (or three by three photons) simultaneously and are not excited. Therefore, the use of multiple photons ensures that the fluorophores are activated only in the focal plane, thus reducing background fluorescence and phototoxicity[124,125].

Sofroniew et al.[126] used the two-photon design to simultaneously record GCaMPs signals from a circular FOV with 5mm radius, reaching depths of up to 1mm. This was used to simultaneously monitor the activity from somatosensory, parietal and motor cortical areas in head-fixed, behaving mice. At the same time, the high spatial resolution permitted the visualization of calcium signals from individual spines. In order to further increase the FOV, Yang et al.[127] introduced the “MATRIEX” design for multiarea two-photon imaging. MATRIEX uses multiple water-immersed miniature objectives, each having its own focal plane. Importantly, the images from these objectives can be simultaneously observed through one low-magnification dry objective. The use of several miniature objectives permitted not only simultaneous imaging from distant brain areas, but also the ability to adjust the imaging depth of each region independently. This was used to simultaneously record GCaMP fluorescence from multiple brain regions distributed across an area up to 12mm^2 and located at different depths: primary visual cortex (V1), primary motor cortex (M1) and CA1 region of hippocampus. Wagner and colleagues used two independent two-photon systems to image calcium activity from L5 of premotor cortex and cerebellum granule cells (GrCs) with single cell spatial resolution[128]. The experiment was conducted on awake head-restrained mice and allowed the researchers to examine the activity patterns in L5 and GrCs during a motor learning task. In order to use multiphoton imaging in freely moving animals, miniature versions of two-photon microscopes were recently developed[129-131]. Zong et al.[131] used mini two-photon microscopes for calcium imaging in V1 in freely moving mice while keeping the spatial resolution at the level of individual spines, which is comparable to the conventional design. More recently, Klioutchnikov et al. adopted a three-photon design for a head-mounted version and performed cortical imaging to a depth of 1.1 mm in freely moving rats with a spatial resolution of a few micrometers, enabling imaging of calcium signals from single soma and dendrites[132].

Despite these technical advances, both conventional multiphoton and confocal methods are point-scanning techniques. Therefore, they have a speed acquisition limit which is set by the fluorescence lifetime of the fluorophore and the pulse of the laser. In other words, one can proceed with the next scanning point of the specimen only after the signal from the previous point is fully acquired. This limitation could be overcome by performing multiple scans in parallel, therefore, performing multispot multiphoton imaging (see Figure 2 for details)[133,134]. However, the parallel scanning of multiple spots requires spreading the laser beam to excite multiple spots in parallel, which reduces the excitation intensity at each individual spot, potentially compromising the fluorophore excitation. This constraint cannot be simply overcome by increasing the laser power due to excessive heating of the tissue. An increase in the excitation intensity in the multispot two-photon design can be achieved by combining two-photon imaging with light sheet microscopy[135,136]. The light sheet microscopy approach uses a side illumination that increases the chance of a photon being absorbed by the fluorophore in the desired plane (e.g. increased photon yield) while reducing photobleaching and phototoxicity, since it uses less laser power in comparison to confocal and multiphoton approaches. Photon light sheet fluorescent calcium imaging has been used for *in-vivo* functional imaging in awake head-restrained mice. However, it still has limited FOV (340x650µm) and depth (135µm), which restricted the analysis to only the motor cortex[137]. *In-vivo* two-photon light sheet imaging[135,136,138,139] has not yet been applied for wide field imaging in mice or rats. However, taking into account the rapid technical advances in multiphoton imaging, we anticipate that the combination of a two-photon setup and light sheet microscopy will soon be implemented to further increase the FOV of functional fluorescent imaging.

Intrinsic Optical Imaging

Despite being one of the most widely used methods for *in-vivo* wide field fluorescent brain imaging, the use of artificial fluorophores (e.g. GCaMPs) is inevitably linked with either invasive interventions such as microinjections or with genetically modified organisms[109]. This impedes the application of these methods to other experimental animals (e.g. non-human primates) and humans. Intrinsic Optical Imaging (IOI)[106,140] relies on the difference in light absorption between oxygenated and deoxygenated haemoglobin and provides a non-invasive alternative to fluorescent imaging. In brief, oxygenated haemoglobin (HbO_2) has lower absorption at 630nm in comparison to deoxygenated haemoglobin (HbR). This decreased absorption leads to higher reflectance, which can be detected by an optical system. The opposite effect occurs at 480nm, where HbO_2 has higher absorption in comparison to HbR. The absorption at 530nm or 590nm is insensitive to the oxygenated state of haemoglobin and is used to assess changes in haemoglobin concentration (HbT)[141]. State-of-the art IOI use standard charged coupled device (CCD) cameras to collect the reflected light, while the illumination source at a specific wavelength can be achieved with LEDs or filters applied to a white light source[141].

The first application of IOI in neuroscience was by Grinvald and colleagues in 1986[106]. In their work, IOI with light at a wavelength of 665 to 750 nm was used to map the activation of the exposed barrel cortex in anesthetized rats during mechanical stimulation of whiskers. In the same study, IOI was used to map orientational columns in the visual cortex of cats and monkeys, highlighting a potential implementation of IOS in cross-species research.

Over the years, IOI has been adapted for imaging in the entire cortex in rodents[142,143]. White et al. used IOI to study resting state functional connectivity in the dorsal cortex in anesthetized mice with a FOV of 1 cm^2 across the exposed intact skull[143]. Specifically, they used multiple LEDs (478 nm, 588 nm, 610 nm and 625 nm) to simultaneously acquire signals of both HbO_2 and HbR and used these patterns for functional parcellation of the mouse cortex. Kura and colleagues later compared the resting state cortical connectivity maps based on IOS from multiple wavelengths versus those obtained from a single wavelength. The results revealed that connectivity maps based on IOS from HbO_2 and HbR are quantitatively comparable with the maps based on HbT changes[142].

However, conventional IOI has some fundamental constraints. Since IOI is based on the hemodynamic response, it lacks cell-type specificity and has limited temporal resolution compared to other optical methods. Furthermore, like all optical imaging methods, it suffers from limitations in spatial resolution due to signal scattering by the skull. In experiments where non-invasiveness is not a necessary parameter, IOI can be combined with other imaging techniques (eg calcium imaging), bypassing these limitations. For example, researchers from Hillman's lab measured the IOS and GCaMP fluorescent signal from bilaterally exposed dorsal cortex in awake, head-fixed mice[141]. The simultaneous assessment of IOS and fluorescent signals, named Wide Field Optical Mapping (WFOM), allowed an increase in spatial resolution after correcting for the cross-talk between the excitation and emission spectra of GCaMP and the absorption of oxygenated and deoxygenated haemoglobin. Ultimately, it was possible to achieve single-cell resolution, with cell type-specificity ensured by the GCaMP expression.

Light scattering imaging

In the Fluorescence Imaging section, we have focused on practical approaches that rely on measurements of absorbed light. However, the interaction of light with the sample (i.e. the brain) is not limited to absorption and is also affected by scattering. In the following section we will briefly discuss light scattered imaging. We limit our focus to two areas: (1) light scattering mechanisms and their influence on IOS and (2) Laser Speckle Imaging.

Mechanisms of light scattering and its influence on IOS.

As summarized by Villinger and Chance[144], there are two types of light scattering associated with neural activity: *fast* and *slow*. In 1980 Tasaki, Iwasa and Gibbons[145] described the physiological basis of *fast scattering*. They used a photon sensor located on the surface of a claw nerve to detect motion of the nerve surface upon travelling of an action potential *in-vitro*. As shown later[144], this movement of the cell membrane leads to changes in the refractive index of the membrane, which ultimately affect the scattering of light. In the early 1990s MacVircar and Hochman studied the mechanism of *slow scattering* by measuring light transmission in the dendritic area of the CA1 region in slices of rat brain. Synaptic activity has been found to result in increased light transmission. This effect was related to the potential glial swelling triggered by the increased extracellular concentration of K+, which occurred during the generation of an action potential. The swelling of the cells causes less light scattering, therefore, increasing light transmission[146]. This could not be explained by changes in HbO2 absorbance [146,147], thus exposing a mainly different factor that affects IOS.

The “fast” and “slow” scatterings were further confirmed by *in-vivo* rodent experiments. Rector and colleagues[148] recorded IOS from the barrel cortex of anaesthetized rats. Using a specifically designed fiber optic probe[149] that was placed on top of the dura matter, they measured fluctuations in scattered light intensity on a millisecond time scale upon twitching of the whisker. The data from “fast scattered” light was further used to map the individual columns in the barrel cortex. Subsequently, Pan et al.[150] were able to simultaneously measure two effects that drive IOS upon spontaneous neuronal activation: (1) the increased absorption driven by increased HbO_2 concentration (2) the reduction of overall neural tissue scattering caused by neural tissue swelling. In Brief, Pan and colleagues used two implantable optodes (i.e. a fibre pair): the light source and the detector, to measure the light transmission through the neural tissue of anaesthetized rats. The pair of fibres was used to measure from either primary somatosensory area or caudate putamen. Importantly, both effects: absorption by HbO_2 and scattering by swelled tissue, were on the same timescale – seconds, emphasizing the interference between *slow scattering* and IOS. This interference can lead to a potential misinterpretation of the imaging results. One of the possible solutions to circumvent this pitfall is the one suggested by Pan et al. simultaneous measurement of light absorption and scattering. Finally, the underlying physiology of *slow scattering* and *fast scattering* is independent from neurovascular coupling suggesting scattering as a separate

imaging contrast[148,150]. Despite the current limitation to a single area of the brain, the potential use of, for example, different pairs of fibers may allow for in vivo "imaging" from multiple brain areas.

Laser Speckle Imaging

In addition to the *static scattering*, in which particle motion is ignored, light scattering is also used for CBF quantification in Laser Speckle Contrast Imaging (LSCI). In short, if coherent light -such as from a laser- is scattered on moving particles -such as red blood cells- the resulting interference patterns, or speckles, will cause a dynamic change in the backscattered light.

In 1981, Ferchner and Briers [151] suggested making a short exposure (in the 10 millisecond interval[152]) of the speckle temporal fluctuations, thus converting the unknown distribution of the velocities to the variations of the speckle contrast. These contrast changes were then converted into intensity distributions, which reflect the velocity distribution of the moving particles. This approach established a basis for LSCI's CBF visualization. In the early 2000s Dunn and colleagues[152] were the first to use LSCI to measure CBF in anesthetized rats. The researchers used a CCD camera through the 6x6 mm FOV of the cortex of rats suffering from diffuse cortical depression or cerebral ischemia. The spatio-temporal resolution was 10 µm and 1 ms, respectively. In 2020 Postnov and colleagues [153] monitored CBF after stroke induction in mice with an exposure time of approximately 30µs and a spatial temporal resolution of 10 µm and 10 µs. Importantly, LSCI is currently used for clinical research in several fields of medicine, including neurology[154]. This increases the translational potential of this technique, which could in the near future lead to a general acceptance of LSCI as the standard for CBF monitoring in neurosurgery.

Photoacoustic imaging

Despite recent methodological breakthroughs, non-invasive *in vivo* optical microscopy still faces inherent optical limitations that restrict it to mostly cortical investigations[155]. To this end, photoacoustic (optoacoustic) imaging (PAI) offers high resolution in tissue depths far beyond current microscopy standards while maintaining rich optical contrast[156,157]. In PAI, signal generation relies on the absorption of pulsed laser light at specific optical wavelengths by endogenous chromophores like oxy-/deoxy-haemoglobin or exogenous contrast agents. Tissue heating due to the process of photon absorption produces broadband acoustic waves at megahertz frequencies (photoacoustic effect) which can be detected at the tissue surface by ultrasound transducers and reconstructed based on the distribution of absorbed optical energy[156]. While PAI's prevailing application is in cancer research[158,159], its non-invasive nature and ability to directly monitor biological processes make it an appealing tool for *in vivo* neuroimaging. The following part will review the most recent applications of PAI in wide-field functional imaging in rodents.

Photoacoustic visualization of in vivo neural dynamics

Given that PAI combines both optical excitation and acoustic detection, a variety of imaging techniques are available, with photoacoustic microscopy (PAM) and tomography (PAT) being the most promising ones for pre-clinical *in vivo* functional neuroimaging (see[160] for a comprehensive overview of PAI methods).

Photoacoustic microscopy

PAM operates by scanning a tightly focused laser beam point-by-point across the tissue surface and detecting the thermoelastically evoked acoustic waves[161]. It provides a comprehensive and quantitative characterization of cerebral hemodynamics with excellent spatial resolution of a few microns[162]. An early application of PAM verified the 'initial dip' of the BOLD-fMRI hemodynamic response to an

electric stimulus as rapid changes in arteriolar oxy-/deoxy-haemoglobin ratios[163]. PAM systems have since been further developed and used for many applications in neuroscience[155,164,165]. Using acoustic-resolution PAM (AR-PAM), Stein et al.[166] non-invasively imaged blood-oxygenation dynamics of several cortical vessels in rodents during controlled hypoxia and hyperoxia challenges. Follow-up systems, capable of three-dimensional high-speed imaging, were introduced a few years after to non-invasively map cortical blood-oxygenation at the capillary level[161,167,168]. Modern PAM systems now enable the investigation of spontaneous cerebral hemodynamic fluctuations and their associated functional connections in rodent research[164,169]. With contrast enhancing agents like genetically-encoded chromophores and voltage sensitive dyes (VSD), the repertoire of PAI was extended to not only include the detection of hemodynamic processes but also direct detection and quantification of neuronal activity[170,171]. For example, Shemetov et al.[172] engineered a genetically encoded calcium indicator with an increase up to 600% in the fluorescence response to calcium. The probe was validated *in vivo* using hybrid photoacoustic and light sheet microscopy, where both neuronal and hemodynamic activity could be captured with high resolution through the intact mouse skull. Despite constant technical advances, though, PAM's high resolution and imaging speed are yet to be applicable to tissue penetration depths beyond 1 mm. In such cases, photoacoustic tomographic systems based on ring-shaped transducer arrays can provide deep brain volumetric visualization of hemodynamics and stimulus-evoked brain activity[155,160,173].

Photoacoustic tomography

PAT uses several wavelength lasers to evoke photoacoustic waves, making it possible to non-invasively and volumetrically measure varying concentrations of endogenous chromophores and exogenous contrast agents in deep brain tissue[174-176]. In fact, the first *in vivo* photoacoustic images of small animals were re-constructed based on PAT system scans from a rat's head: Wang et al.[177] accurately mapped brain structures with and without lesions, as well as functional cerebral hemodynamic changes in cortical blood vessels around the barrel cortex in response to whisker stimulation. PAT has also been successfully applied to study whole-brain hemodynamics[176] and even resting-state functional connectivity in rodents[178]. In 2016, Tang et al.[179,180] described a similar but wearable cap-like PAT system for awake and behaving rats, with a high in-plane spatial resolution of 200µm at depths of up to 11 mm. In a mouse model of epilepsy, an oxy-/deoxy-haemoglobin based photoacoustic computed tomography (PACT) scanning system captured the superficial epileptic wave spreading around the epileptic focus and a corresponding wave propagating in the opposite hemisphere[181]. Going beyond superficial cortical measurements, a newly devised system combining PACT and electrophysiological recordings enabled the first non-invasive visualization of real-time thalamo-cortical activity during an epileptic seizure in the whole mouse brain. Furthermore, endogenous contrast based PACT successfully mapped brain-wide activation during electrical fore- and hindpaw stimulation in mice to their somatosensory cortex forelimb and hindlimb areas, respectively[182]. Using contrast enhancement, Gottschalk et al.[183] recently measured real-time *in vivo* calcium transients across the mouse brain by devising a functional PA neuro-tomography setup. They reached sufficient sensitivity to directly detect fast neural responses to electrical hindpaw stimulation. Using a near infrared VSD, Kang et al.[184] monitored *in vivo* chemically evoked seizures in rats at sub-mm spatial resolution, without the need for invasive craniotomy of skull thinning.

Although still in its infancy, whole-brain functional PAI has rapidly evolved in recent years to meet the standards of the mainstay neuroimaging methods. With its multiscale imaging capabilities comprising rich optical contrast, high spatial resolution and imaging rate, PAI sits at a unique position to directly visualize key parameters of brain function. While PAI does come with its own set of limitations, much

like any other neuroimaging technique, it nevertheless shows great potential to bridge the gap between micro- and macroscopic functional neuroimaging.

Conclusions

Until recently, the inability to measure brain activity in its entirety and simultaneously link it to physiologically relevant processes has limited our understanding of the relationship between neuronal activity and complex cognitive processes. This has changed dramatically with new large-scale functional imaging methods, which allow us to study previously invisible processes both in real time and longitudinally, and to associate these processes with healthy or impaired neural function.

In this review, we have seen how the development of these approaches has allowed for higher spatial resolution, a wider field of view, and greater temporal resolution. However, there are still many limitations of these techniques that prevent a full understanding of local and global brain dynamics and their impact on behavior and cognition. We have outlined some of these gaps in each section of this review to guide current and future investigators.

Besides precise measurement of neural activity, the field of functional imaging also requires integration with computational models capable of using this data in order to make predictions about behavioral functions, which can then be tested experimentally. However, this has not been addressed here to give greater emphasis to the technical / experimental aspect of the methods discussed. The challenge for the future is therefore not only to design and engineer systems capable of detecting brain functions with the highest possible precision and accuracy, but also to integrate and analyze this data within theoretical models to develop a complete picture that can guide our understanding of the human brain. This review aims to attract new researchers to help unravel the mysteries of large-scale neural activity.

Competing interests

The authors declare no competing interests.

Acknowledgment

This work was supported by a SNSF AMBIZIONE PZ00P3_173984/1 grant to V.Z. and by an ETH Grant (ETH-25 18-2) to V.Z. M.M. is supported by research grant ETH-38 16-2.

Figure legends

Adapted versions of the figures from [140,185-189] were used in Figure 2 and Graphical Abstract.

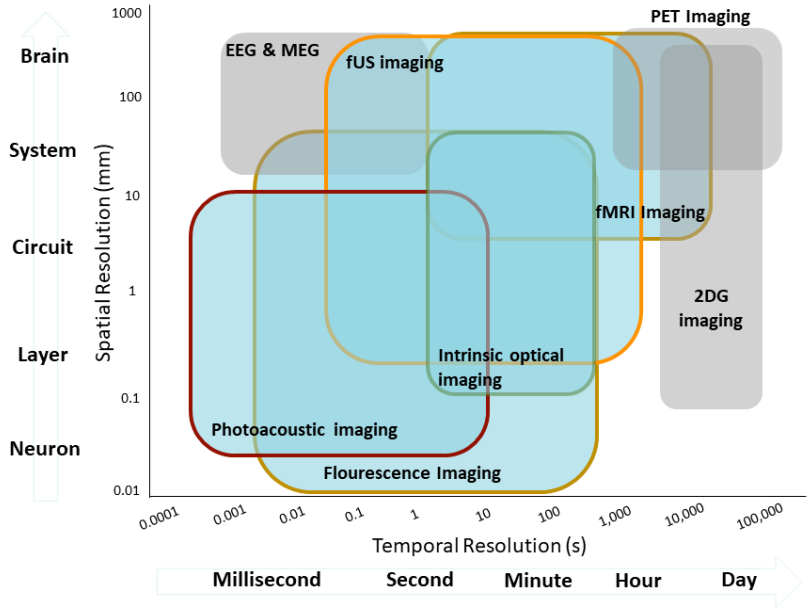

Figure 1. The spatiotemporal overview of imaging techniques used for studying rodent whole-brain function. Each coloured box represents approximate spatiotemporal scope of the labelled technique. Light blue coloured boxes represent techniques covered in this review, while grey boxes techniques not covered. EEG, electroencephalography; MEG, magnetoencephalography; PET, positron emission tomography; 2-DG, 2-deoxyglucose; fUS, functional ultrasound; fMRI, functional magnetic resonance imaging.

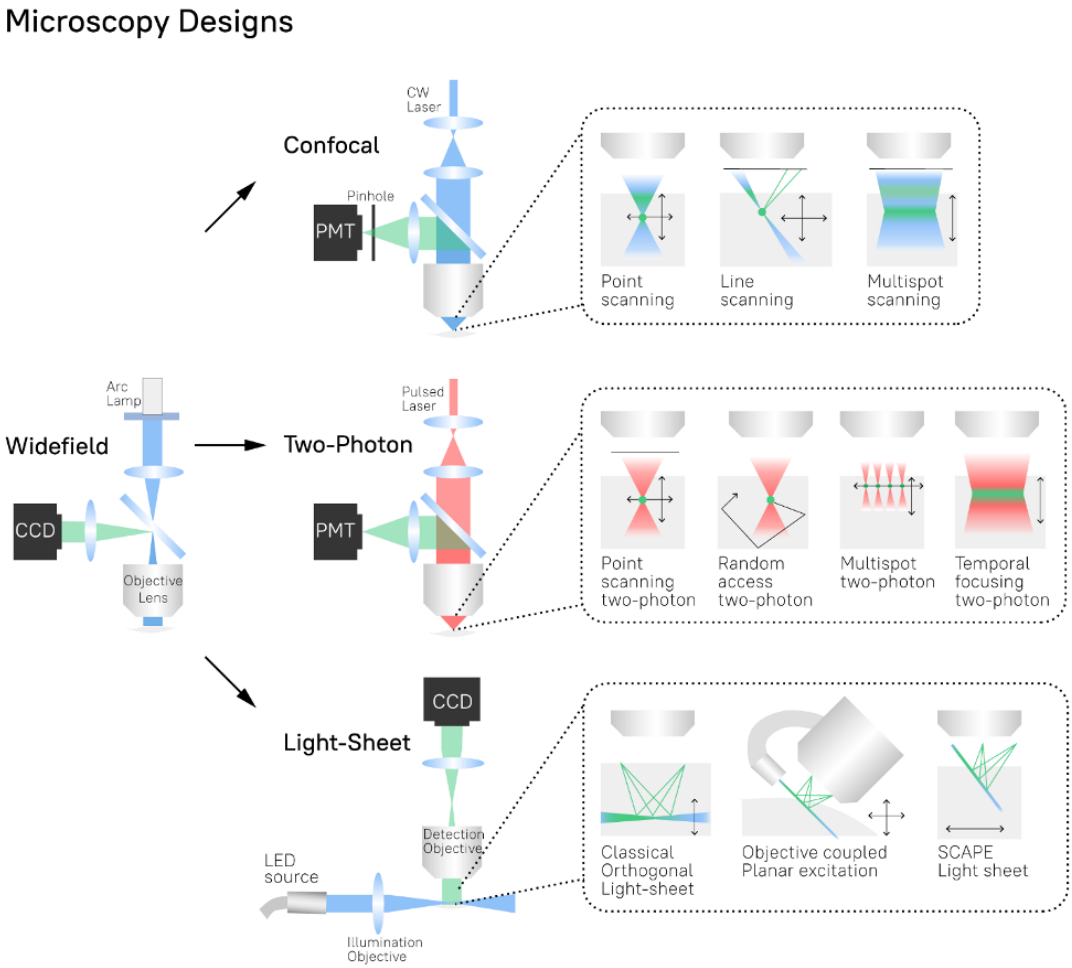

Figure 2. Microscopy Designs. The main engineering components and operational modes of Widefield, Confocal, Two-Photon and Light-Sheet microscopes. Abbreviations: Light Emitting Diode -LED, Charge-Coupled Device-CCD

Widefield microscopes use Arc Lamps or LEDs (not shown) to produce a beam of light at a specific wavelength. In the case of Arc Lamps filters (horizontal blue bulk) are used to select a specific wavelength from a continuous spectrum. The illumination light irradiates the entire specimen through the objective lens causing the excitation of fluorophores. The fluorescent signal emitted during the luminescence process is collected by the same objective lens and reflected by the dichroic mirror (deflected blue bulk) toward the CCD camera. **Confocal microscopes** use the same optical system as a widefield microscope, with a few differences: (i) lasers are used as a light source, (ii) a "pinhole" is used to cut off the light outside of the focal plane and (iii) a Photo-Multiplier Tube (PMT) is used for image acquisition. Continuous Wave Lasers (CW Laser) are typically used in confocal designs ensuring the stable amplitude and wavelength of the illumination light. Depending on the operational mode the illumination is focused on the specific point (point-scanning), line (line-scanning) or multiple points (multisport scanning) inside a specimen. The black arrows feature possible scanning directions. The emitted fluorescent light is passed through the pinhole and ultimately collected by the PMT, which enhances the amplitude of the impingement light.

Note that scanning mechanisms (XY) are not shown and that the confocal pinhole would need to be placed in the descanned pathway. When featured, XY scanner (e.g. galvo mirror scanner) is located on the detection pathway between the objective and dichroic mirror. Z-steppers or Tunable Acoustic Gradient (TAG) lens for z-scanning are also not shown. When depicted, they are located at the back

focal aperture of the objective. **Multiphoton microscopes** are represented by the example of the two-photon design. It utilizes the same components as the confocal, but with two principal differences: (i) a pulsed laser is used, (ii) a "pinhole" is not required. Two-photon microscopy is based on the two-photon excitation process: a fluorophore simultaneously absorbs two photons that together bring sufficient energy to cause the fluorophore excitation. Subsequent relaxation of the excited fluorophore back to the ground state is accompanied by the fluorescence emission. For the practical realization of the simultaneous absorption of two photons, a pulsed laser produces a beam of photons with the energy tuned for the two-photon excitation process of the targeted fluorophore: ½ of the excitation energy per photon. Since only the fluorophores at the focal plane can simultaneously absorb two photons, a pinhole is not used. Two-photon microscopes can be used in various scanning modes. Point scanning mode refers to an illumination of a single point per scanning session. Random access is the point scanning mode which is used for a set of predefined locations in the sample. Therefore, the random access technique does not image the whole specimen, but rather the part sufficient for the analysis. During a multispot session multiple points are illuminated in parallel during the same scanning session. Finally, during the temporal focusing the laser beam impinges on the diffraction grid, producing several beams that are further guided by the optical system to constructively interfere in the focal plane located at the specimen. Thus, the two-photon temporal focusing mode leads to the activation of a single plane. **Light sheet microscopes** typically use an LED (or several) to illuminate the specimen from the side. Such illumination process is called "Oblique Illumination". Emitted fluorescent signal is captured by the objective lens and further transmitted to the CCD camera. Classical Orthogonal Light-Sheet Microscopy uses two orthogonal objectives: the first is for illumination and the second is for detection. This design requires a highly constrained sample geometry and either physical sample translation for 3D imaging or complex synchronization of illumination and detection planes. Both constraints limit the acquisition speed of Classical Orthogonal Light-Sheet Microscopy. In the Objective Coupled Planar Excitation (OCPE) design the position of the illumination and detection objectives are mechanically coupled. Despite the ensured alignment of the illumination and detection planes, OCPE still requires mechanical movement of the coupled objectives to perform scanning. Finally, SCAPE microscopy acquires images using an angled, swept light sheet in a single objective. SCAPE permits completely translationless three-dimensional imaging of intact samples at rates exceeding 20 volumes per second.

References

1 Lakatos, P., Gross, J. & Thut, G. A New Unifying Account of the Roles of Neuronal Entrainment. *Current Biology* **29**, R890-R905, doi:https://doi.org/10.1016/j.cub.2019.07.075 (2019).

2 Houweling, A. R. & Brecht, M. Behavioural report of single neuron stimulation in somatosensory cortex. *Nature* **451**, 65-68, doi:10.1038/nature06447 (2008).

3 Elsayed, G. F. & Cunningham, J. P. Structure in neural population recordings: an expected byproduct of simpler phenomena? *Nat Neurosci* **20**, 1310-1318, doi:10.1038/nn.4617 (2017).

4 Gao, P. & Ganguli, S. On simplicity and complexity in the brave new world of large-scale neuroscience. *Curr Opin Neurobiol* **32**, 148-155, doi:10.1016/j.conb.2015.04.003 (2015).

5 Gallego, J. A. *et al.* Cortical population activity within a preserved neural manifold underlies multiple motor behaviors. *Nature Communications* **9**, 4233, doi:10.1038/s41467-018-06560-z (2018).

6 Sporns, O., Tononi, G. & Kötter, R. The human connectome: A structural description of the human brain. *PLoS Comput Biol* **1**, e42, doi:10.1371/journal.pcbi.0010042 (2005).

7 Ogawa, S., Lee, T. M., Kay, A. R. & Tank, D. W. Brain magnetic resonance imaging with contract dependent on blood oxygenation. *Proceedings of the National Academy of Sciences of the United States of America* **87**, 9868-9872 (1990).

8 ME, R. & MA, M. Brain work and brain imaging. *Annual review of neuroscience* **29**, doi:10.1146/annurev.neuro.29.051605.112819 (2006).

9 D, K. *et al.* A guide to delineate the logic of neurovascular signaling in the brain. *Frontiers in neuroenergetics* **3**, doi:10.3389/fnene.2011.00001 (2011).

10 B, C. & E, H. Revisiting the role of neurons in neurovascular coupling. *Frontiers in neuroenergetics* **2**, doi:10.3389/fnene.2010.00009 (2010).

11 RB, B., VE, G., AB, S., F, M. & A, S. Variability of the coupling of blood flow and oxygen metabolism responses in the brain: a problem for interpreting BOLD studies but potentially a new window on the underlying neural activity. *Frontiers in neuroscience* **8**, doi:10.3389/fnins.2014.00139 (2014).

12 E, A., AW, C., Y, X., JM, L. & TH, M. Optogenetic stimulation of GABA neurons can decrease local neuronal activity while increasing cortical blood flow. *Journal of cerebral blood flow and metabolism : official journal of the International Society of Cerebral Blood Flow and Metabolism* **35**, doi:10.1038/jcbfm.2015.140 (2015).

13 Ay, N. & Polani, D. Information flows in causal networks. *Advances in Complex Systems*, doi:10.1142/S0219525908001465 (2008).

14 A, D. *et al.* Suppressed neuronal activity and concurrent arteriolar vasoconstriction may explain negative blood oxygenation level-dependent signal. *The Journal of neuroscience : the official journal of the Society for Neuroscience* **27**, doi:10.1523/JNEUROSCI.0134-07.2007 (2007).

15 Desjardins, M. *et al.* Awake Mouse Imaging: From Two-Photon Microscopy to Blood Oxygen Level–Dependent Functional Magnetic Resonance Imaging. *Biological Psychiatry: Cognitive Neuroscience and Neuroimaging* **4**, 533-542, doi:https://doi.org/10.1016/j.bpsc.2018.12.002 (2019).

16 Devor, A. *et al.* Neurovascular Imaging. *Frontiers in Neuroenergetics* **4**, doi:10.3389/fnene.2012.00001 (2012).

17 H, U. *et al.* Cell type specificity of neurovascular coupling in cerebral cortex. *eLife* **5**, doi:10.7554/eLife.14315 (2016).

18 Kim, S.-G. & Ogawa, S. Biophysical and Physiological Origins of Blood Oxygenation Level-Dependent fMRI Signals. *Journal of Cerebral Blood Flow & Metabolism* **32**, 1188-1206, doi:10.1038/jcbfm.2012.23 (2012).

19 Gore, J. C. Principles and practice of functional MRI of the human brain. *Journal of Clinical Investigation* **112**, 4-9, doi:10.1172/jci200319010 (2003).

20 Bharat Biswal, F. Z. Y., Victor M. Haughton, James S. Hyde. Functional Connectivity in the Motor Cortex of Resting Human Brain Using Echo-Planar MRI. *Magnetic Resonance in Medicine* **34**, 537-541 (1995).

21 Fox, M. D. & Raichle, M. E. Spontaneous fluctuations in brain activity observed with functional magnetic resonance imaging. *Nat Rev Neurosci* **8**, 700-711, doi:10.1038/nrn2201 (2007).

22 M, M. & J, L. Gradient echo imaging. *Journal of magnetic resonance imaging : JMRI* **35**, doi:10.1002/jmri.23638 (2012).

23 PA, B. Selection of the optimal pulse sequence for functional MRI - Oxford Scholarship. doi:10.1093/acprof:oso/9780192630711.003.0006 (2021).

24 JL, B., LM, H., BR, R. & RM, W. MR contrast due to intravascular magnetic susceptibility perturbations. *Magnetic resonance in medicine* **34**, doi:10.1002/mrm.1910340412 (1995).

25 Zhao, F., Wang, P. & Kim, S. G. Cortical depth-dependent gradient-echo and spin-echo BOLD fMRI at 9.4T. *Magn Reson Med* **51**, 518-524, doi:10.1002/mrm.10720 (2004).

26 Keilholz, S. D., Silva, A. C., Raman, M., Merkle, H. & Koretsky, A. P. BOLD and CBV-weighted functional magnetic resonance imaging of the rat somatosensory system. *Magn Reson Med* **55**, 316-324, doi:10.1002/mrm.20744 (2006).

27 Zhao, F., Zhao, T., Zhou, L., Wu, Q. & Hu, X. BOLD study of stimulation-induced neural activity and resting-state connectivity in medetomidine-sedated rat. *NeuroImage* **39**, 248-260, doi:10.1016/j.neuroimage.2007.07.063 (2008).

28 Pawela, C. P. *et al.* Resting-state functional connectivity of the rat brain. *Magnetic resonance in medicine* **59**, 1021-1029, doi:10.1002/mrm.21524 (2008).

29 Zhang, F. *et al.* Optogenetic interrogation of neural circuits: technology for probing mammalian brain structures. *Nat Protoc* **5**, 439-456, doi:10.1038/nprot.2009.226 (2010).

30 Hutchison, R. M., Mirsattari, S. M., Jones, C. K., Gati, J. S. & Leung, L. S. Functional networks in the anesthetized rat brain revealed by independent component analysis of resting-state FMRI. *J Neurophysiol* **103**, 3398-3406, doi:10.1152/jn.00141.2010 (2010).

31 Jonckers, E., Van Audekerke, J., De Visscher, G., Van der Linden, A. & Verhoye, M. Functional connectivity fMRI of the rodent brain: comparison of functional connectivity networks in rat and mouse. *PLoS One* **6**, e18876, doi:10.1371/journal.pone.0018876 (2011).

32 Sforazzini, F., Schwarz, A. J., Galbusera, A., Bifone, A. & Gozzi, A. Distributed BOLD and CBV-weighted resting-state networks in the mouse brain. *Neuroimage* **87**, 403-415, doi:10.1016/j.neuroimage.2013.09.050 (2014).

33 Zerbi, V., Grandjean, J., Rudin, M. & Wenderoth, N. Mapping the mouse brain with rs-fMRI: An optimized pipeline for functional network identification. *Neuroimage* **123**, 11-21, doi:10.1016/j.neuroimage.2015.07.090 (2015).

34 Lu, H. *et al.* Rat brains also have a default mode network. *Proceedings of the National Academy of Sciences* **109**, 3979-3984, doi:10.1073/pnas.1200506109 (2012).

35 Jonckers, E. *et al.* Different anesthesia regimes modulate the functional connectivity outcome in mice. *Magnetic Resonance in Medicine* **72**, 1103-1112, doi:https://doi.org/10.1002/mrm.24990 (2014).

36 Liang, Z., Liu, X. & Zhang, N. Dynamic resting state functional connectivity in awake and anesthetized rodents. *NeuroImage* **104**, 89-99, doi:https://doi.org/10.1016/j.neuroimage.2014.10.013 (2015).

37 Nasrallah, F. A., Tay, H. C. & Chuang, K. H. Detection of functional connectivity in the resting mouse brain. *Neuroimage* **86**, 417-424, doi:10.1016/j.neuroimage.2013.10.025 (2014).

38 Paasonen, J., Stenroos, P., Salo, R. A., Kiviniemi, V. & Grohn, O. Functional connectivity under six anesthesia protocols and the awake condition in rat brain. *Neuroimage* **172**, 9-20, doi:10.1016/j.neuroimage.2018.01.014 (2018).

39 Grandjean, J. *et al.* Common functional networks in the mouse brain revealed by multi-centre resting-state fMRI analysis. *Neuroimage* **205**, 116278, doi:10.1016/j.neuroimage.2019.116278 (2020).

40 Grandjean, J. *et al.* Dynamic reorganization of intrinsic functional networks in the mouse brain. *Neuroimage* **152**, 497-508, doi:10.1016/j.neuroimage.2017.03.026 (2017).

41 Sethi, S. S., Zerbi, V., Wenderoth, N., Fornito, A. & Fulcher, B. D. Structural connectome topology relates to regional BOLD signal dynamics in the mouse brain. *Chaos* **27**, 047405, doi:10.1063/1.4979281 (2017).

42 Belloy, M. E. *et al.* Dynamic resting state fMRI analysis in mice reveals a set of Quasi-Periodic Patterns and illustrates their relationship with the global signal. *Neuroimage* **180**, 463-484, doi:10.1016/j.neuroimage.2018.01.075 (2018).

43 Liska, A., Galbusera, A., Schwarz, A. J. & Gozzi, A. Functional connectivity hubs of the mouse brain. *Neuroimage* **115**, 281-291, doi:10.1016/j.neuroimage.2015.04.033 (2015).

44 Bertero, A. *et al.* Autism-associated 16p11.2 microdeletion impairs prefrontal functional connectivity in mouse and human. *Brain* **141**, 2055-2065, doi:10.1093/brain/awy111 (2018).

45 Oh, S. W. *et al.* A mesoscale connectome of the mouse brain. *Nature* **508**, 207-214, doi:10.1038/nature13186 (2014).

46 Grandjean, J., Zerbi, V., Balsters, J. H., Wenderoth, N. & Rudin, M. Structural Basis of Large-Scale Functional Connectivity in the Mouse. *J Neurosci* **37**, 8092-8101, doi:10.1523/jneurosci.0438-17.2017 (2017).

47 Mills, B. D. *et al.* Correlated Gene Expression and Anatomical Communication Support Synchronized Brain Activity in the Mouse Functional Connectome. *J Neurosci* **38**, 5774-5787, doi:10.1523/jneurosci.2910-17.2018 (2018).

48 Schlegel, F. *et al.* Fiber-optic implant for simultaneous fluorescence-based calcium recordings and BOLD fMRI in mice. *Nat Protoc* **13**, 840-855, doi:10.1038/nprot.2018.003 (2018).

49 Wang, M., He, Y., Sejnowski, T. J. & Yu, X. Brain-state dependent astrocytic Ca(2+) signals are coupled to both positive and negative BOLD-fMRI signals. *Proc Natl Acad Sci U S A* **115**, E1647-e1656, doi:10.1073/pnas.1711692115 (2018).

50 Tong, C. *et al.* Differential coupling between subcortical calcium and BOLD signals during evoked and resting state through simultaneous calcium fiber photometry and fMRI. *Neuroimage* **200**, 405-413, doi:10.1016/j.neuroimage.2019.07.006 (2019).

51 Lake, E. M. R. *et al.* Simultaneous cortex-wide fluorescence Ca(2+) imaging and whole-brain fMRI. *Nat Methods* **17**, 1262-1271, doi:10.1038/s41592-020-00984-6 (2020).

52 Schulz, K. *et al.* Simultaneous BOLD fMRI and fiber-optic calcium recording in rat neocortex. *Nat Methods* **9**, 597-602, doi:10.1038/nmeth.2013 (2012).

53 Zerbi, V. *et al.* Resting-State Functional Connectivity Changes in Aging apoE4 and apoE-KO Mice. *The Journal of Neuroscience* **34**, 13963, doi:10.1523/JNEUROSCI.0684-14.2014 (2014).

54 Grandjean, J. *et al.* Early Alterations in Functional Connectivity and White Matter Structure in a Transgenic Mouse Model of Cerebral Amyloidosis. *The Journal of Neuroscience* **34**, 13780, doi:10.1523/JNEUROSCI.4762-13.2014 (2014).

55 Grandjean, J. *et al.* Complex interplay between brain function and structure during cerebral amyloidosis in APP transgenic mouse strains revealed by multi-parametric MRI comparison. *NeuroImage* **134**, 1-11, doi:https://doi.org/10.1016/j.neuroimage.2016.03.042 (2016).

56 Errico, F. *et al.* A role for D-aspartate oxidase in schizophrenia and in schizophrenia-related symptoms induced by phencyclidine in mice. *Translational Psychiatry* **5**, e512-e512, doi:10.1038/tp.2015.2 (2015).

57 Buehlmann, D., Grandjean, J., Xandry, J. & Rudin, M. Longitudinal resting-state functional magnetic resonance imaging in a mouse model of metastatic bone cancer reveals distinct functional reorganizations along a developing chronic pain state. *PAIN* **159**, 719-727, doi:10.1097/j.pain.0000000000001148 (2018).

58 Sforazzini, F. *et al.* Altered functional connectivity networks in acallosal and socially impaired BTBR mice. *Brain Struct Funct* **221**, 941-954, doi:10.1007/s00429-014-0948-9 (2016).

59 Liska, A. *et al.* Homozygous Loss of Autism-Risk Gene CNTNAP2 Results in Reduced Local and Long-Range Prefrontal Functional Connectivity. *Cereb Cortex* **28**, 1141-1153, doi:10.1093/cercor/bhx022 (2018).

60 Zerbi, V. *et al.* Dysfunctional Autism Risk Genes Cause Circuit-Specific Connectivity Deficits With Distinct Developmental Trajectories. *Cerebral Cortex*, doi:10.1093/cercor/bhy046 (2018).

61 Zerbi, V. *et al.* Inhibiting mGluR5 activity by AFQ056/Mavoglurant rescues circuit-specific functional connectivity in Fmr1 knockout mice. *Neuroimage* **191**, 392-402, doi:10.1016/j.neuroimage.2019.02.051 (2019).

62 Stafford, J. M. *et al.* Large-scale topology and the default mode network in the mouse connectome. *Proceedings of the National Academy of Sciences of the United States of America* **111**, 18745-18750, doi:10.1073/pnas.1404346111 (2014).

63 Balsters, J. H., Zerbi, V., Sallet, J., Wenderoth, N. & Mars, R. B. Primate homologs of mouse cortico-striatal circuits. *eLife* **9**, e53680, doi:10.7554/eLife.53680 (2020).

64 Stenroos, P. *et al.* Awake Rat Brain Functional Magnetic Resonance Imaging Using Standard Radio Frequency Coils and a 3D Printed Restraint Kit. *Frontiers in Neuroscience* **12**, doi:10.3389/fnins.2018.00548 (2018).

65 Liu, Y. *et al.* An open database of resting-state fMRI in awake rats. *NeuroImage* **220**, 117094, doi:https://doi.org/10.1016/j.neuroimage.2020.117094 (2020).

66 Kim, S.-G. *et al.* Cerebral blood volume MRI with intravascular superparamagnetic iron oxide nanoparticles. *NMR Biomed* **26**, 949-962, doi:10.1002/nbm.2885 (2013).

67 Barbier, E. L., Lamalle, L. & Decorps, M. Methodology of Brain Perfusion Imaging *Journal of Magnetic Resonance Imaging* **13**, 496-520 (2001).

68 Wirestam, R. Using contrast agents to obtain maps of regional perfusion and capillary wall permeability. *Imaging in Medicine* **4**, 423-442 (2012).

69 Giorgi, A. *et al.* Brain-wide Mapping of Endogenous Serotonergic Transmission via Chemogenetic fMRI. *Cell Rep* **21**, 910-918, doi:10.1016/j.celrep.2017.09.087 (2017).

70 Grandjean, J. *et al.* A brain-wide functional map of the serotonergic responses to acute stress and fluoxetine. *Nat Commun* **10**, 350, doi:10.1038/s41467-018-08256-w (2019).

71 Lee, H.-L., Li, Z., Coulson, E. J. & Chuang, K.-H. Ultrafast fMRI of the rodent brain using simultaneous multi-slice EPI. *NeuroImage* **195**, 48-58, doi:https://doi.org/10.1016/j.neuroimage.2019.03.045 (2019).

72 Jung, W. B., Im, G. H., Jiang, H. & Kim, S. G. Early fMRI responses to somatosensory and optogenetic stimulation reflect neural information flow. *Proc Natl Acad Sci U S A* **118**, doi:10.1073/pnas.2023265118 (2021).

73 MacKinnon, M. J., Song, S., H.,L-M., Lee, S-H., Johnson G. A., Shih, I. Y-Y.,. in *Proceedings of the International Society for Magnetic Resonance in Medicine (ISMRM)* Vol. 28 (Wiley, 2020).

74 Le Bihan, D., Urayama, S.-i., Aso, T., Hanakawa, T. & Fukuyama, H. Direct and fast detection of neuronal activation in the human brain with diffusion MRI. *Proceedings of the National Academy of Sciences* **103**, 8263, doi:10.1073/pnas.0600644103 (2006).

75 Abe, Y., Tsurugizawa, T. & Le Bihan, D. Water diffusion closely reveals neural activity status in rat brain loci affected by anesthesia. *PLOS Biology* **15**, e2001494, doi:10.1371/journal.pbio.2001494 (2017).

76 Andrew, R. D., Jarvis, C. R. & Obeidat, A. S. Potential Sources of Intrinsic Optical Signals Imaged in Live Brain Slices. *Methods* **18**, 185-196, doi:https://doi.org/10.1006/meth.1999.0771 (1999).

77 Abe, Y., Van Nguyen, K., Tsurugizawa, T., Ciobanu, L. & Le Bihan, D. Modulation of water diffusion by activation-induced neural cell swelling in Aplysia Californica. *Scientific Reports* **7**, 6178, doi:10.1038/s41598-017-05586-5 (2017).

78 Nunes, D., Gil, R. & Shemesh, N. A rapid-onset diffusion functional MRI signal reflects neuromorphological coupling dynamics. *Neuroimage* **231**, 117862, doi:10.1016/j.neuroimage.2021.117862 (2021).

79 Aso, T., Urayama, S.-i., Fukuyama, H. & Le Bihan, D. Comparison of diffusion-weighted fMRI and BOLD fMRI responses in a verbal working memory task. *NeuroImage* **67**, 25-32, doi:https://doi.org/10.1016/j.neuroimage.2012.11.005 (2013).

80 De Luca, A., Schlaffke, L., Siero, J. C. W., Froeling, M. & Leemans, A. On the sensitivity of the diffusion MRI signal to brain activity in response to a motor cortex paradigm. *Human Brain Mapping* **40**, 5069-5082, doi:https://doi.org/10.1002/hbm.24758 (2019).

81 Nunes, D., Ianus, A. & Shemesh, N. Layer-specific connectivity revealed by diffusion-weighted functional MRI in the rat thalamocortical pathway. *Neuroimage* **184**, 646-657, doi:10.1016/j.neuroimage.2018.09.050 (2019).

82 Jasanoff, A. Bloodless FMRI. *Trends Neurosci* **30**, 603-610, doi:10.1016/j.tins.2007.08.002 (2007).

83 Bartelle, B. B., Barandov, A. & Jasanoff, A. Molecular fMRI. *J Neurosci* **36**, 4139-4148, doi:10.1523/JNEUROSCI.4050-15.2016 (2016).

84 Ghosh, S., Harvey, P., Simon, J. C. & Jasanoff, A. Probing the brain with molecular fMRI. *Curr Opin Neurobiol* **50**, 201-210, doi:10.1016/j.conb.2018.03.009 (2018).

85 Hsieh, V. & Jasanoff, A. Bioengineered probes for molecular magnetic resonance imaging in the nervous system. *ACS Chem Neurosci* **3**, 593-602, doi:10.1021/cn300059r (2012).

86 Lee, T., Cai, L. X., Lelyveld, V. S., Hai, A. & Jasanoff, A. Molecular-Level Functional Magnetic Resonance Imaging of Dopaminergic Signaling. *Science* **344**, 533, doi:10.1126/science.1249380 (2014).

87 Li, N. & Jasanoff, A. Local and global consequences of reward-evoked striatal dopamine release. *Nature* **580**, 239-244, doi:10.1038/s41586-020-2158-3 (2020).

88 Just, N. Proton functional magnetic resonance spectroscopy in rodents. *NMR Biomed* **34**, e4254, doi:10.1002/nbm.4254 (2021).

89 Rhodes, C. J. Magnetic resonance spectroscopy. *Sci Prog* **100**, 241-292, doi:10.3184/003685017X14993478654307 (2017).

90 Mace, E. *et al.* Functional ultrasound imaging of the brain: theory and basic principles. *IEEE Trans Ultrason Ferroelectr Freq Control* **60**, 492-506, doi:10.1109/tuffc.2013.2592 (2013).

91 Evans, H. D. M. W. N. *Doppler Ultrasound: Physics, Instrumentation and Signal Processing*. (Wiley, 2000).

92 LaRovere, K. L. Transcranial Doppler ultrasound in children with stroke and cerebrovascular disorders. *Curr Opin Pediatr* **27**, 712-718, doi:10.1097/mop.0000000000000282 (2015).

93 Deffieux, T., Demene, C., Pernot, M. & Tanter, M. Functional ultrasound neuroimaging: a review of the preclinical and clinical state of the art. *Current Opinion in Neurobiology* **50**, 128-135, doi:https://doi.org/10.1016/j.conb.2018.02.001 (2018).

94 Macé, E. *et al.* Functional ultrasound imaging of the brain. *Nat Methods* **8**, 662-664, doi:10.1038/nmeth.1641 (2011).

95 Urban, A. *et al.* Chronic assessment of cerebral hemodynamics during rat forepaw electrical stimulation using functional ultrasound imaging. *Neuroimage* **101**, 138-149, doi:10.1016/j.neuroimage.2014.06.063 (2014).

96 Rideau , A. B. N. *et al.* Transcriptomic regulations in oligodendroglial and microglial cells related to brain damage following fetal growth restriction. *Glia* **64**, 2306-2320, doi:10.1002/glia.23079 (2016).

97 Osmanski, B.-F., Pezet, S., Ricobaraza, A., Lenkei, Z. & Tanter, M. Functional ultrasound imaging of intrinsic connectivity in the living rat brain with high spatiotemporal resolution. *Nature Communications* **5**, 5023, doi:10.1038/ncomms6023 (2014).

98 Tiran, E. *et al.* Transcranial Functional Ultrasound Imaging in Freely Moving Awake Mice and Anesthetized Young Rats without Contrast Agent. *Ultrasound Med Biol* **43**, 1679-1689, doi:10.1016/j.ultrasmedbio.2017.03.011 (2017).

99 Macé, É. *et al.* Whole-Brain Functional Ultrasound Imaging Reveals Brain Modules for Visuomotor Integration. *Neuron* **100**, 1241-1251.e1247, doi:https://doi.org/10.1016/j.neuron.2018.11.031 (2018).

100 Errico, C. *et al.* Ultrafast ultrasound localization microscopy for deep super-resolution vascular imaging. *Nature* **527**, 499-502, doi:10.1038/nature16066 (2015).

101 Errico, C. *et al.* Transcranial functional ultrasound imaging of the brain using microbubble-enhanced ultrasensitive Doppler. *Neuroimage* **124**, 752-761, doi:10.1016/j.neuroimage.2015.09.037 (2016).

102 Dana, H. *et al.* High-performance calcium sensors for imaging activity in neuronal populations and microcompartments. *Nature Methods*, doi:10.1038/s41592-019-0435-6 (2019).

103 Chen, T. W. *et al.* Ultrasensitive fluorescent proteins for imaging neuronal activity. *Nature*, doi:10.1038/nature12354 (2013).

104 Choi, M., Kwok, S. J. J. & Yun, S. H. in *Physiology* (2015).

105 Paredes, R. M., Etzler, J. C., Watts, L. T., Zheng, W. & Lechleiter, J. D. Chemical calcium indicators. *Methods*, doi:10.1016/j.ymeth.2008.09.025 (2008).

106 Grinvald, A., Lieke, E., Frostig, R. D., Gilbert, C. D. & Wiesel, T. N. Functional architecture of cortex revealed by optical imaging of intrinsic signals. *Nature*, doi:10.1038/324361a0 (1986).

107 Bando, Y., Grimm, C., Cornejo, V. H. & Yuste, R. in *BMC Biology* (2019).

108 Oh, J., Lee, C. & Kaang, B. K. in *Korean Journal of Physiology and Pharmacology* (2019).

109 Russell, J. T. in *British Journal of Pharmacology* (2011).
110 Kuhn, B. & Roome, C. J. in *Frontiers in Cellular Neuroscience* (2019).
111 Miyawaki, A. *et al.* Fluorescent indicators for Ca2+ based on green fluorescent proteins and calmodulin. *Nature*, doi:10.1038/42264 (1997).
112 Piatkevich, K. D. *et al.* Population imaging of neural activity in awake behaving mice. *Nature*, doi:10.1038/s41586-019-1641-1 (2019).
113 Rossi, L. F., Wykes, R. C., Kullmann, D. M. & Carandini, M. Focal cortical seizures start as standing waves and propagate respecting homotopic connectivity. *Nature Communications*, doi:10.1038/s41467-017-00159-6 (2017).
114 Kim, T. H. *et al.* Long-Term Optical Access to an Estimated One Million Neurons in the Live Mouse Cortex. *Cell Reports*, doi:10.1016/j.celrep.2016.12.004 (2016).
115 Peters, A., Fabre, J., Steinmetz, N., Harris, K. & Carandini, M. Striatal activity topographically reflects cortical activity. *Nature* (2021).
116 Ziv, Y. & Ghosh, K. K. in *Current Opinion in Neurobiology* (2015).
117 Malvaut, S., Constantinescu, V. S., Dehez, H., Doric, S. & Saghatelyan, A. in *Frontiers in Neuroscience* (2020).
118 Hamel, E. J. O., Grewe, B. F., Parker, J. G. & Schnitzer, M. J. in *Neuron* (2015).
119 Gonzalez, W. G., Zhang, H., Harutyunyan, A. & Lois, C. Persistence of neuronal representations through time and damage in the hippocampus. *Science*, doi:10.1126/science.aav9199 (2019).
120 de Groot, A. *et al.* Ninscope, a versatile miniscope for multi-region circuit investigations. *eLife*, doi:10.7554/eLife.49987 (2020).
121 Webb, R. H., Hughes, G. W. & Delori, F. C. Confocal scanning laser ophthalmoscope. *Appl Opt* **26**, 1492-1499, doi:10.1364/AO.26.001492 (1987).
122 Yoshida, E. *et al.* In vivo wide-field calcium imaging of mouse thalamocortical synapses with an 8 K ultra-high-definition camera. *Scientific Reports*, doi:10.1038/s41598-018-26566-3 (2018).
123 Dussaux, C. *et al.* in *Optics InfoBase Conference Papers* (2018).
124 Yang, W. & Yuste, R. in *Nature Methods* (2017).
125 Denk, W., Strickler, J. H. & Webb, W. W. Two-photon laser scanning fluorescence microscopy. *Science*, doi:10.1126/science.2321027 (1990).
126 Sofroniew, N. J., Flickinger, D., King, J. & Svoboda, K. A large field of view two-photon mesoscope with subcellular resolution for in vivo imaging. *eLife*, doi:10.7554/eLife.14472 (2016).
127 Yang, M. *et al.* MATRIEX imaging: multiarea two-photon real-time in vivo explorer. *Light: Science and Applications*, doi:10.1038/s41377-019-0219-x (2019).
128 Wagner, M. J. *et al.* Shared Cortex-Cerebellum Dynamics in the Execution and Learning of a Motor Task. *Cell*, doi:10.1016/j.cell.2019.02.019 (2019).
129 Helmchen, F., Denk, W. & Kerr, J. N. D. Miniaturization of two-photon microscopy for imaging in freely moving animals. *Cold Spring Harbor Protocols*, doi:10.1101/pdb.top078147 (2013).
130 Helmchen, F., Fee, M. S., Tank, D. W. & Denk, W. A miniature head-mounted two-photon microscope: High-resolution brain imaging in freely moving animals. *Neuron*, doi:10.1016/S0896-6273(01)00421-4 (2001).
131 Zong, W. *et al.* Fast high-resolution miniature two-photon microscopy for brain imaging in freely behaving mice. *Nature Methods*, doi:10.1038/nmeth.4305 (2017).
132 Klioutchnikov, A. *et al.* Three-photon head-mounted microscope for imaging deep cortical layers in freely moving rats. *Nature Methods*, doi:10.1038/s41592-020-0817-9 (2020).

133 Cheng, L.-C. *et al.* Spatiotemporal focusing-based widefield multiphoton microscopy for fast optical sectioning. *Optics Express*, doi:10.1364/oe.20.008939 (2012).
134 Katona, G. *et al.* Fast two-photon in vivo imaging with three-dimensional random-access scanning in large tissue volumes. *Nature Methods*, doi:10.1038/nmeth.1851 (2012).
135 Hillman, E. M. C., Voleti, V., Li, W. & Yu, H. in *Annual Review of Neuroscience* (2019).
136 Truong, T. V., Supatto, W., Koos, D. S., Choi, J. M. & Fraser, S. E. Deep and fast live imaging with two-photon scanned light-sheet microscopy. *Nature Methods*, doi:10.1038/nmeth.1652 (2011).
137 Bouchard, M. B. *et al.* Swept confocally-aligned planar excitation (SCAPE) microscopy for high-speed volumetric imaging of behaving organisms. *Nature Photonics*, doi:10.1038/nphoton.2014.323 (2015).
138 Maioli, V. *et al.* Fast in vivo multiphoton light-sheet microscopy with optimal pulse frequency. *Biomedical Optics Express*, doi:10.1364/boe.400113 (2020).
139 Schrödel, T., Prevedel, R., Aumayr, K., Zimmer, M. & Vaziri, A. Brain-wide 3D imaging of neuronal activity in Caenorhabditis elegans with sculpted light. *Nature Methods*, doi:10.1038/nmeth.2637 (2013).
140 Hillman, E. M. C. Optical brain imaging in vivo: techniques and applications from animal to man. *Journal of Biomedical Optics*, doi:10.1117/1.2789693 (2007).
141 Ma, Y. *et al.* in *Philosophical Transactions of the Royal Society B: Biological Sciences* (2016).
142 Kura, S. *et al.* Intrinsic optical signal imaging of the blood volume changes is sufficient for mapping the resting state functional connectivity in the rodent cortex. *Journal of Neural Engineering*, doi:10.1088/1741-2552/aaafe4 (2018).
143 White, B. R. *et al.* Imaging of functional connectivity in the mouse brain. *PLoS ONE*, doi:10.1371/journal.pone.0016322 (2011).
144 Villringer, A. & Chance, B. Non-invasive optical spectroscopy and imaging of human brain function. *Trends Neurosci* **20**, 435-442, doi:10.1016/s0166-2236(97)01132-6 (1997).
145 Tasaki, I., Iwasa, K. & Gibbons, R. C. Mechanical changes in crab nerve fibers during action potentials. *Jpn J Physiol* **30**, 897-905, doi:10.2170/jjphysiol.30.897 (1980).
146 MacVicar, B. A. & Hochman, D. Imaging of synaptically evoked intrinsic optical signals in hippocampal slices. *J Neurosci* **11**, 1458-1469 (1991).
147 Andrew, R. D. & MacVicar, B. A. Imaging cell volume changes and neuronal excitation in the hippocampal slice. *Neuroscience* **62**, 371-383, doi:10.1016/0306-4522(94)90372-7 (1994).
148 Rector, D. M., Carter, K. M., Volegov, P. L. & George, J. S. Spatio-temporal mapping of rat whisker barrels with fast scattered light signals. *NeuroImage*, doi:10.1016/j.neuroimage.2005.02.030 (2005).
149 Rector, D. M., Rogers, R. F. & George, J. S. A focusing image probe for assessing neural activity in vivo. *J Neurosci Methods* **91**, 135-145, doi:10.1016/s0165-0270(99)00088-6 (1999).
150 Pan, W. J. *et al.* Detection of neural light-scattering activity in vivo: optical transmittance studies in the rat brain. *Neuroimage* **179**, 207-214, doi:10.1016/j.neuroimage.2018.06.039 (2018).
151 Fercher, A. F. & Briers, J. D. Flow Visualization by Means of Single-Exposure Speckle Photography. *Opt Commun* **37**, 326-330, doi:Doi 10.1016/0030-4018(81)90428-4 (1981).

152 Dunn, A. K., Bolay, H., Moskowitz, M. A. & Boas, D. A. Dynamic imaging of cerebral blood flow using laser speckle. *J Cereb Blood Flow Metab* **21**, 195-201, doi:10.1097/00004647-200103000-00002 (2001).

153 Postnov, D. D., Tang, J., Erdener, S. E., Kilic, K. & Boas, D. A. Dynamic light scattering imaging. *Sci Adv* **6**, doi:10.1126/sciadv.abc4628 (2020).

154 Richards, L. M. *et al.* Intraoperative multi-exposure speckle imaging of cerebral blood flow. *J Cereb Blood Flow Metab* **37**, 3097-3109, doi:10.1177/0271678X16686987 (2017).

155 Ntziachristos, V. Going deeper than microscopy: the optical imaging frontier in biology. *Nat Methods* **7**, 603-614, doi:10.1038/nmeth.1483 (2010).

156 Wang, L. V. & Yao, J. A practical guide to photoacoustic tomography in the life sciences. *Nat Methods* **13**, 627-638, doi:10.1038/nmeth.3925 (2016).

157 Zackrisson, S., van de Ven, S. M. W. Y. & Gambhir, S. S. Light in and sound out: emerging translational strategies for photoacoustic imaging. *Cancer Res* **74**, 979-1004, doi:10.1158/0008-5472.CAN-13-2387 (2014).

158 Laufer, J. *et al.* In vivo preclinical photoacoustic imaging of tumor vasculature development and therapy. *J Biomed Opt* **17**, 056016, doi:10.1117/1.JBO.17.5.056016 (2012).

159 Levi, J. *et al.* Molecular photoacoustic imaging of follicular thyroid carcinoma. *Clin Cancer Res* **19**, 1494-1502, doi:10.1158/1078-0432.CCR-12-3061 (2013).

160 Deán-Ben, X. L., Gottschalk, S., Mc Larney, B., Shoham, S. & Razansky, D. Advanced optoacoustic methods for multiscale imaging of in vivo dynamics. *Chem Soc Rev* **46**, 2158-2198, doi:10.1039/c6cs00765a (2017).

161 Maslov, K., Zhang, H. F., Hu, S. & Wang, L. V. Optical-resolution photoacoustic microscopy for in vivo imaging of single capillaries. *Opt Lett* **33**, 929-931, doi:10.1364/ol.33.000929 (2008).

162 Ovsepian, S. V., Olefir, I., Westmeyer, G., Razansky, D. & Ntziachristos, V. Pushing the Boundaries of Neuroimaging with Optoacoustics. *Neuron* **96**, 966-988, doi:10.1016/j.neuron.2017.10.022 (2017).

163 Liao, L. D. *et al.* Transcranial imaging of functional cerebral hemodynamic changes in single blood vessels using in vivo photoacoustic microscopy. *J Cereb Blood Flow Metab* **32**, 938-951, doi:10.1038/jcbfm.2012.42 (2012).

164 Chen, Z. *et al.* Multifocal structured illumination optoacoustic microscopy. *Light: Science & Applications* **9**, 1-9, doi:doi:10.1038/s41377-020-00390-9 (2020).

165 Liu, Y. *et al.* Aggregation-Induced Absorption Enhancement for Deep Near-Infrared II Photoacoustic Imaging of Brain Gliomas In Vivo. *Adv Sci (Weinh)* **6**, 1801615, doi:10.1002/advs.201801615 (2019).

166 Stein, E. W., Maslov, K. & Wang, L. V. Noninvasive, in vivo imaging of blood-oxygenation dynamics within the mouse brain using photoacoustic microscopy. *J Biomed Opt* **14**, 020502-020502, doi:10.1117/1.3095799 (2009).

167 Yao, J. *et al.* High-speed label-free functional photoacoustic microscopy of mouse brain in action. *Nature Methods* **12**, 407-410, doi:doi:10.1038/nmeth.3336 (2015).

168 Hu, S., Maslov, K., Tsytsarev, V. & Wang, L. V. Functional transcranial brain imaging by optical-resolution photoacoustic microscopy. doi:Hu, Song and Maslov, Konstantin and Tsytsarev, Vassiliy and Wang, Lihong V. (2009) Functional transcranial brain imaging by optical-resolution photoacoustic microscopy. Journal of Biomedical Optics, 14 (4). Art. No. 040503. ISSN 1083-3668. PMCID PMC2855841. https://resolver.caltech.edu/CaltechAUTHORS:20160920-160445234 <https://resolver.caltech.edu/CaltechAUTHORS:20160920-160445234> (2009).

169 Hariri, A. *et al.* in *Photons Plus Ultrasound: Imaging and Sensing 2016.* 97085A (International Society for Optics and Photonics).
170 Giepmans, B. N., Adams, S. R., Ellisman, M. H. & Tsien, R. Y. The fluorescent toolbox for assessing protein location and function. *Science* **312**, 217-224, doi:10.1126/science.1124618 (2006).
171 Chudakov, D. M., Matz, M. V., Lukyanov, S. & Lukyanov, K. A. Fluorescent proteins and their applications in imaging living cells and tissues. *Physiol Rev* **90**, 1103-1163, doi:10.1152/physrev.00038.2009 (2010).
172 Shemetov, A. A. *et al.* A near-infrared genetically encoded calcium indicator for in vivo imaging. *Nature Biotechnology*, 1-10, doi:doi:10.1038/s41587-020-0710-1 (2020).
173 Ku, G. & Wang, L. V. Deeply penetrating photoacoustic tomography in biological tissues enhanced with an optical contrast agent. *Opt Lett* **30**, 507-509, doi:10.1364/ol.30.000507 (2005).
174 Wang, L. V. & Gao, L. Photoacoustic microscopy and computed tomography: from bench to bedside. *Annu Rev Biomed Eng* **16**, 155-185, doi:10.1146/annurev-bioeng-071813-104553 (2014).
175 Li, L. *et al.* Label-free photoacoustic tomography of whole mouse brain structures. *Neurophotonics* **3**, 035001, doi:10.1117/1.NPh.3.3.035001 (2016).
176 Yao, J. *et al.* Noninvasive photoacoustic computed tomography of mouse brain metabolism in vivo. *Neuroimage* **64**, 257-266, doi:10.1016/j.neuroimage.2012.08.054 (2013).
177 Wang, X. *et al.* Noninvasive laser-induced photoacoustic tomography for structural and functional in vivo imaging of the brain. *Nat Biotechnol* **21**, 803-806, doi:10.1038/nbt839 (2003).
178 Nasiriavanaki, M. *et al.* High-resolution photoacoustic tomography of resting-state functional connectivity in the mouse brain. *Proc Natl Acad Sci U S A* **111**, 21-26, doi:10.1073/pnas.1311868111 (2014).
179 Tang, J., Coleman, J. E., Dai, X. & Jiang, H. Wearable 3-D Photoacoustic Tomography for Functional Brain Imaging in Behaving Rats. *Sci Rep* **6**, 25470, doi:10.1038/srep25470 (2016).
180 Tang, J., Dai, X. & Jiang, H. Wearable scanning photoacoustic brain imaging in behaving rats. *J Biophotonics* **9**, 570-575, doi:10.1002/jbio.201500311 (2016).
181 Zhang, P. *et al.* High-resolution deep functional imaging of the whole mouse brain by photoacoustic computed tomography in vivo. *J Biophotonics* **11**, doi:10.1002/jbio.201700024 (2018).
182 Avanaki, M. R. N. *et al.* in *Photons Plus Ultrasound: Imaging and Sensing 2013.* 85813K (International Society for Optics and Photonics).
183 Gottschalk, S., Fehm, T. F., Deán-Ben, X. L., Tsytsarev, V. & Razansky, D. Correlation between volumetric oxygenation responses and electrophysiology identifies deep thalamocortical activity during epileptic seizures. *Neurophotonics* **4**, 011007, doi:10.1117/1.NPh.4.1.011007 (2017).
184 J, K. *et al.* Transcranial Recording of Electrophysiological Neural Activity in the Rodent Brain in vivo Using Functional Photoacoustic Imaging of Near-Infrared Voltage-Sensitive Dye. *Frontiers in neuroscience* **13**, doi:10.3389/fnins.2019.00579 (2019).
185 Hillman, E. M. C. *et al.* High-speed 3D imaging of cellular activity in the brain using axially-extended beams and light sheets. *Current Opinion in Neurobiology* **50**, 190-200, doi:10.1016/j.conb.2018.03.007 (2018).
186 Mannam, V., Zhang, Y., Yuan, X., Ravasio, C. & Howard, S. S. in *JPhys Photonics* (2020).

187 Chen, X. *et al.* Sensory evoked fMRI paradigms in awake mice. *NeuroImage* **204**, 116242, doi:https://doi.org/10.1016/j.neuroimage.2019.116242 (2020).

188 Chelini, G. *et al.* Aberrant Somatosensory Processing and Connectivity in Mice Lacking Engrailed-2. *J Neurosci* **39**, 1525-1538, doi:10.1523/JNEUROSCI.0612-18.2018 (2019).

189 Lee, C., Park, S., Kim, J. & Kim, C. in *Handbook of Photonics for Biomedical Engineering* (eds Aaron Ho-Pui Ho, Donghyun Kim, & Michael G. Somekh) 247-269 (Springer Netherlands, 2017).